Optical and Electrical Characterisation of a 3D-printed Luminescent Solar Concentrator

*Richard Capener, Jake Manning, Piotr Itrych, Sara J. Baldock and Lefteris Danos**

Department of Chemistry, Energy Lancaster, Lancaster University, Lancaster, LA1 4YB, UK

**Email: l.danos@lancaster.ac.uk*

Keywords

Luminescent Solar Concentrator, 3D printing, Perylene Red Dye, Indoor Photovoltaics, Solar Cells.

Abstract

A Luminescent Solar Concentrator (LSC) was fabricated using stereolithography (SLA) 3D printing by doping a commercially available liquid resin with the widely used Perylene Red dye. The LSC was optically and electrically characterised through optical spectroscopy and current-voltage electrical measurements. Its performance was found to be comparable to that of an injection-moulded LSC with a similar dye concentration. We demonstrated that the transparency of the printed resin improved significantly following a sanding and polishing process, with only minimal bulk scattering contributions, as determined through optical measurements. The approach was successfully scaled up by fabricating a larger LSC, confirming the viability of 3D printing as a flexible and accessible method that enables fast, low-cost fabrication for research-scale LSC development. This is the first demonstration of an LSC fabricated via 3D printing, showing promising results and highlighting the potential of this approach as a flexible research tool for optimising LSC performance.

1 Introduction

Luminescent Solar Concentrators (LSCs) have been a topic of research since their concept was proposed in the late 70s [1–4], due to their potential to capture direct and diffuse light over a large area and concentrate the emitted (luminescence) light onto a smaller area solar cell reducing the cost of solar electricity [5–7]. However, since this original research on LSCs, their areas of application has shifted direction [8]. One of the potential applications for LSCs are in building integrated photovoltaics (BIPV) [9,10]. They can be integrated into buildings almost invisibly, reducing the aesthetic and functional limitations of traditional solar panels. They are insensitive to orientation angle, and their absorption is unaffected by diffuse light caused by cloudy weather. This means that LSCs could help facilitate green architecture as they are suitable for BIPV applications [11,12]. They can be integrated into buildings in the form of transparent panels for indoor PV [13] and internet of things (IoT) applications [14].

LSCs have the potential to serve as efficient light-harvesting components for energy-autonomous systems, enabling the sustainable powering of IoT devices [15]. They can demonstrate self-powered, IoT-connected sensing elements for smart building scenarios. Recent studies have reported LSC-based temperature sensors coupled to photovoltaic cells, where the temperature-dependent emission of the luminophore is exploited and the electrical output is used to estimate temperature. The data are then transmitted wirelessly in real time to an online interface, demonstrating the feasibility of building-integrated devices with intrinsic temperature-sensing capability [16,17]. Such window-relevant LSC demonstrators operating under sunlight and artificial lighting offer a promising route towards net-zero buildings and smart cities. Because of their customisable size and ability to operate efficiently under both indoor and outdoor lighting conditions, LSCs can provide low-maintenance power for sensors, wearable electronics, and smart building applications [18]. Their adjustable optical properties, including colour and transparency, make LSCs well suited for applications requiring both visual appeal and energy generation. Beyond energy harvesting, LSCs have shown potential in optical communication applications, functioning as visible light receivers for free-space data communication systems [19] or for dual-function incorporating photovoltaic and piezoelectric properties for use in self-powered IoT systems and smart devices [20].

An LSC consists of a transparent plate or waveguide doped with a luminescent dye. Light enters through the top surface and is absorbed by the luminescent dye. The absorbed light is emitted at a longer wavelength, and the waveguide directs the light to the edges of the LSC via total internal reflection (TIR) where small area solar cells are attached. There are

two major loss mechanisms in an LSC which are escape-cone losses and reabsorption losses.

The LSC relies on TIR to concentrate light, however, photons absorbed by the luminescent dye are emitted isotropically. The matrix material used for dye doping has a refractive index which defines a critical angle below which light striking the boundary between the material and air will not be reflected but instead refracted and leave the LSC. Using this critical angle, an escape cone (shown in Fig. 1) can be defined within which incident photons are lost from all the surfaces of the LSC. Photons striking the surface with an angle greater than the critical angle which defines the escape cone are trapped and can reach the edge of the LSC unless reabsorbed by the dye.

Photon reabsorption occurs because of partial overlap between the absorption and emission spectra. Some of the emitted photons travelling to the edge of the LSC still have sufficient energy to be absorbed by the luminescent material and hence re-emitted. Because of isotropic emission the problem of escape-cone losses arises again. In addition, the dye may have a non-unity luminescence quantum yield which can further lead to photon losses. Single-dye LSCs are limited in absorbing a large part of the incident solar spectrum. As a result, an effective LSC should exhibit a low probability of reabsorption, a near-unity luminescence quantum yield, and strong absorption of incident light [7,21].

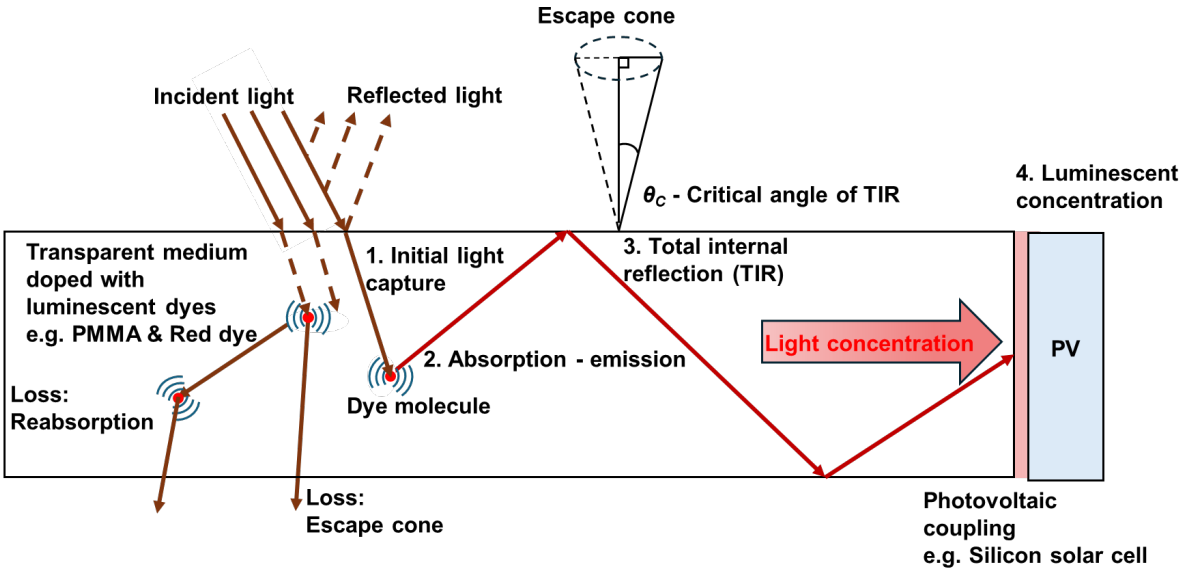

Figure 1. Schematic of the operation of a Luminescent Solar Concentrator (LSC). Light is incident through the front face of the LSC and is absorbed by a luminophore (1). After absorption the dye is excited and undergoes isotropic emission (2). A significant part of the emitted light is trapped via total internal reflection (TIR) (3) and directed to the edge of

the LSC (4) where a solar cell converts the concentrated light to electricity. Two major loss mechanisms are identified as reabsorption and escape-cone losses.

Two popular methods of fabricating LSCs reported in the literature are spin coating [5,22–25] and injection moulding (IM) [26]. Spin coating is used to apply thin films to the surface of a substrate. It is a fast and low-cost technique, allowing for the formation of uniform films with control over the thickness of the film being formed. The main disadvantage of this method is the high amount of waste: only 2-5% of the material dispensed onto the substrate is used to make the film with the rest lost during the spinning process and wasted [27].

Injection moulding is a widely used method for fabricating plastic components. The heated material is injected into a mould and allowed to set. In this process the luminophore is mixed into the host matrix so the dye can disperse within the waveguide. IM fabrication results in little waste, and produces high-quality LSCs and is considered the gold-standard method for LSC manufacturing [28]. However, in a research environment, the need for custom moulds for each shape is costly and time-consuming, which limits rapid iteration and experimental flexibility.

In contrast, 3D printing (additive manufacturing) offers a promising route for lab-scale LSC prototyping and experimentation. It creates physical objects from a CAD drawing through layer-by-layer fabrication. This allows the fabrication of complex and highly detailed shapes that would otherwise be difficult to achieve using conventional methods. Additionally, a range of materials can be printed including plastics, ceramics, and metals [29]. 3D printing is fast, cheap and easily customisable making it particularly useful in the manufacturing industry for making prototypes of new products. It is used worldwide in a range of fields [30], however there is very little evidence in the literature of 3D printing being used to make LSCs [31].

There are limited reports in the literature on the use of 3D printing to fabricate LSCs, primarily due to the poor transparency of printed objects. Without post-processing, a significant portion of the incident light is scattered within the waveguide, resulting in very low optical efficiency. However, recent advances have demonstrated the fabrication of high-quality transparent objects using 3D printing, such as contact lenses produced with digital light processing (DLP) techniques and transparent resins [32,33].

The advantages of 3D printing, including reduced material waste and the ability to easily fabricate bespoke LSC shapes, make it a valuable tool for research. While it may not yet replace industrial-scale manufacturing methods such as injection moulding, 3D printing can

accelerate the development of new LSC designs in the lab, offering a low-barrier route to testing novel geometries, materials, and dye configurations.

In this work, we report the first fabrication of an LSC using a transparent stereolithography resin doped with Perylene Red (Pe-Red). We have developed a two-step process to improve the optical transparency of the 3D-printed LSC plates. We demonstrated the potential of 3D printing by comparing the optical and electrical performance of a small 3D-printed LSC with that of a previously studied IM LSC [34,35]. The performance of the small 3D LSC is comparable to the IM LSC, and we further scaled up the 3D printing to a large LSC to demonstrate the potential of our methodology and stereolithographic printing of LSCs.

2 Materials and Methods

2.1 Materials

Perylene red dye (2,9-Bis(2,6-diisopropylphenyl)-5,6,12,13-tetraphenoxyanthra[2,1,9-def:6,5,10-d'e'f']diisoquinoline-1,3,8,10(2H,9H)-tetraone) was obtained from AmBeed and used as received. Isopropanol (IPA) and toluene were obtained from Sigma Aldrich. The Perylene Red (Pe-Red) dye containing print resin was prepared to the appropriate concentration (g/L) by addition of the dye to a Clear 3D resin (V4 Formlabs, Somerville, MA, USA) followed by ultrasonic dissolution.

2.2 3D printing of Luminescent Solar Concentrators

A stereolithography (SLA) printer that uses a laser to cure a liquid resin was used to fabricate the LSCs. The printer was a desktop SLA printer from Formlabs (Form2, Somerville, MA, USA) equipped with a 405 nm (max 250 mW) laser with a spot size of 140 µm and operates in the inverted SLA mode by employing tanks with optically clear bases and a retracting build platform for layer-by-layer curing.

Two different designs for the LSC plates were fabricated. A small LSC (2.0 cm × 2.0 cm × 0.1 cm) and a large LSC (10.0 cm × 10.0 cm × 0.5 cm) were designed using Fusion 360 CAD software (Autodesk, San Francisco, CA, USA). The drawing files were exported using a standard SLA format (.stl) and imported into the manufacturer's bespoke printer software (PreForm v. 3.42.0.443, Formlabs) which handled the conversion of drawing file to printer commands. The collector plates were printed at the highest resolution layer slicing (z: 25 µm thick). Print jobs were orientated with the LSC side vertically and the print supports were minimised (i.e., build platform base supports were kept to one edge with minimal face support) so as to keep the LSC plate as natively smooth as possible. Standard resin print settings were used; the tank heat setting was 35 °C and the tank wiper was used (i.e., for

print job layer-by-layer detachment) which also ensured that the dye-loaded resin was homogeneously mixed throughout the print run. Typical print times range from under 2 hours (coarser resolution) to about 5 hours (25 μm resolution) for a single LSC, with batches of up to 30 samples printed in under 10 hours.

The optical properties of the 3D-printed Clear Resin V4 [36] are very similar to those of poly(methyl methacrylate) (PMMA), a standard LSC material. The resin, primarily composed of urethane dimethacrylate (UDMA) with methacrylate monomers and a phosphine oxide derivative photoinitiator, forms a highly cross-linked, optically clear polymer with low shrinkage and good stability. It's refractive index (~1.51 across 400–700 nm) closely matches that of PMMA (≈1.49–1.50), and both materials exhibit high transparency and low scattering after polishing. The use of this 3D-printable resin also facilitates rapid prototyping and optimisation of LSC parameters such as dye concentration and geometry.

After printing, the 3D prints were rinsed in isopropyl alcohol(IPA) for 20 mins and dried using a nitrogen gun before removal of the print supports. Dry prints were then wet sanded down using first 1500 grit and then 2000 grit numbered sandpaper. The polishing process includes two stages: 5 minutes of sanding and 10 minutes of final polishing per sample. All sides (front, back and edges) of the LSC were sanded down and it was followed with polishing all sides using a 6'' bench buffer/polisher (Clarke CBB15).

Four solar cells with size 2.1 cm × 0.2 cm (Supercells) were connected in series and attached to a custom-made 3D rig to measure the performance of the small LSCs. To test the performance of the large LSC, four solar cells (SunPower) were cut using a microdrill with dimensions 10.0 cm × 5.0 cm and were attached to the edges of the 3D printed LSC using transparent optical glue (UV LOCA Liquid Clear Adhesive Glue).

2.3 Optical and Electrical Characterisation

All absorption spectra (300 nm − 800nm) were recorded using an Agilent Cary 60 UV/Vis absorption spectrometer. The emission spectra were measured with an Agilent Cary Eclipse spectrometer and the edge fluorescence spectra were recorded with a fibre optic setup using an Avantes 2048 pixel CCD spectrometer Avaspec-2048, grating UA (200 nm – 1100 nm), slit-25μm and Avasoft 7.5 software with a blue LED (Luxeon Star, 465 nm) illumination source.

Current-voltage measurements were performed using a Keithley 2400 source meter controlled by a custom LabVIEW program. The LSCs were placed inside a custom-built enclosure equipped with a solar simulator (AM1.5G, LS0106 150 W Xe light source, Lot-Oriel). For the larger LSCs (10 cm × 10 cm × 0.5 cm), a different measurement setup was

used to accommodate the increased device size and ensure uniform illumination. Current–voltage (I-V) measurements were carried out using a Keithley 2611A source meter operating with the TSP Express software. The LSCs were measured inside a custom-made black enclosure equipped with two strips of white LEDs (NS1, Valoya, 400-700 nm). All measurements were performed under uniform illumination, and the incident light power (37.5 W m^{-1}) was measured using a Macam Q203 Quantum radiometer. A black matte backing was used in all measurements in accordance with standardised LSC characterisation protocols [37].

3 Results and Discussion

3.1 Optical Characterisation

Perylene red dye (Pe Red) was selected as the luminescent material that would be used to fabricate 3D printed LSCs because it is a dye commonly used in the literature for fabrication of small scale prototype LSCs [28,38,39]. It has a high photoluminescence quantum yield (~97%) and good photostability [40]. Figure 2 shows the structure of Pe-Red, an example of absorption/emission spectra of Pe-Red dissolved in toluene, and a series of absorption spectra that were used to estimate the molar absorption coefficient in toluene.

Pe-Red absorbs strongly through π → π* aromatic transitions. Excitation to the first and second excited state energy levels gives rise to the two peaks seen in the absorption spectrum. A Beer-Lambert plot fit found the molar absorption coefficient to be 46,704 ± 109 M^{-1} cm^{-1}. This value matched well with the literature which estimates the molar absorption coefficient to be between 45,300 and 49,900 M^{-1} cm^{-1} [38].

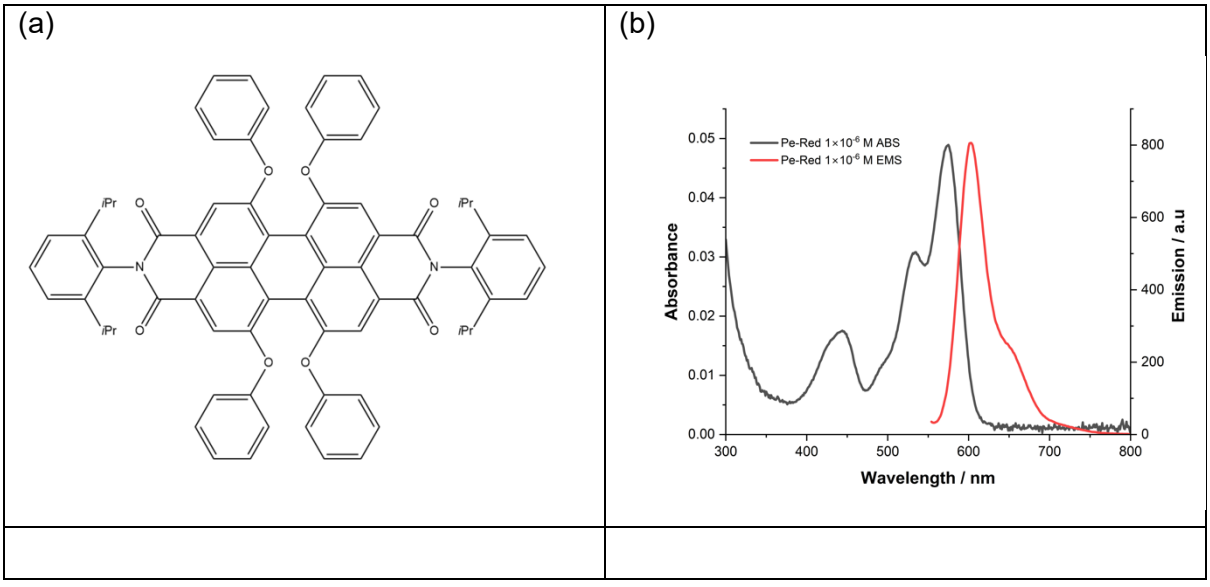

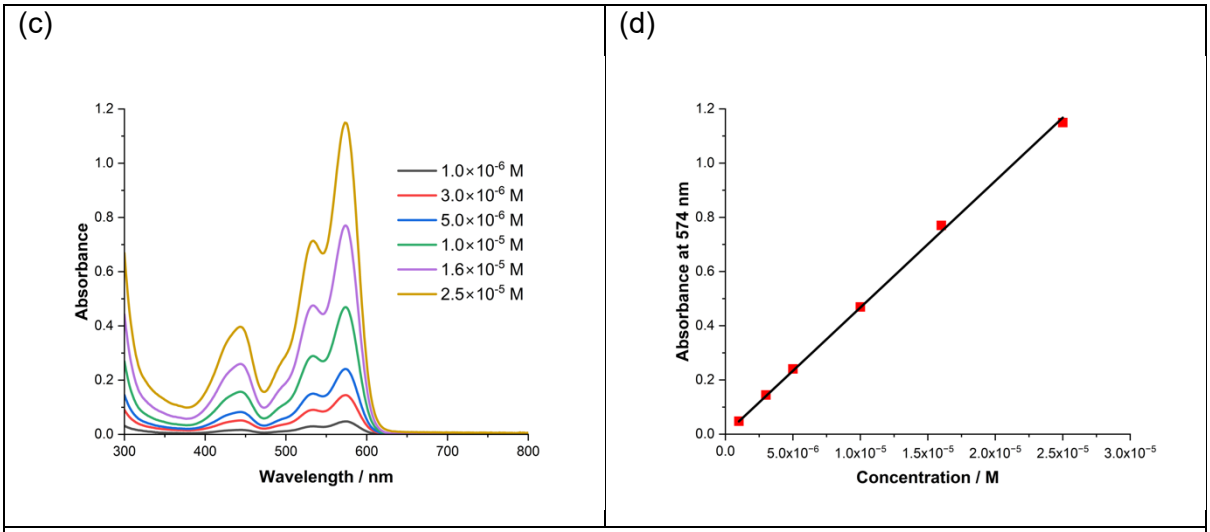

Figure 2. (a) Chemical Structure of Pe-Red used in this work. (b) Absorption and emission spectra of Pe-Red dissolved in toluene. (c) Absorption spectra for Pe-Red for six different concentrations (in toluene). (d) Beer-Lambert plot of concentration *vs* absorbance at a wavelength of 574 nm. The molar absorption coefficient (at 574 nm) is estimated to be 46,704 ± 109 M^{-1} cm^{-1}.

A key factor in improving the performance of 3D printed LSCs is the optical transparency. Figure 3 shows images of 3D printed blank plates with and without a sanding and polishing process. From the transmittance spectrum (Fig. 3b) it is clear that transparency improved significantly after surface treatment. The blank plate achieves transmittance up to 90%. Below 410 nm the absorption of the 3D printed resin is visible.

The SEM images of untreated and treated LSC blank plates are shown in Fig. 3c and Fig. 3d respectively. The images of the untreated LSC plate exhibited features consistent with the layer-by-layer laser curing and lines that result from the nature of the vector printing and other factors due to the printing process (print pauses for automatic tank filling, print peeling off the tank bottom). The sanding first removes the lines caused by 3D printing and the polishing step can smooth the surface. The combination of these two steps leaves the surface clear and transparent with an excellent quality polished finish.

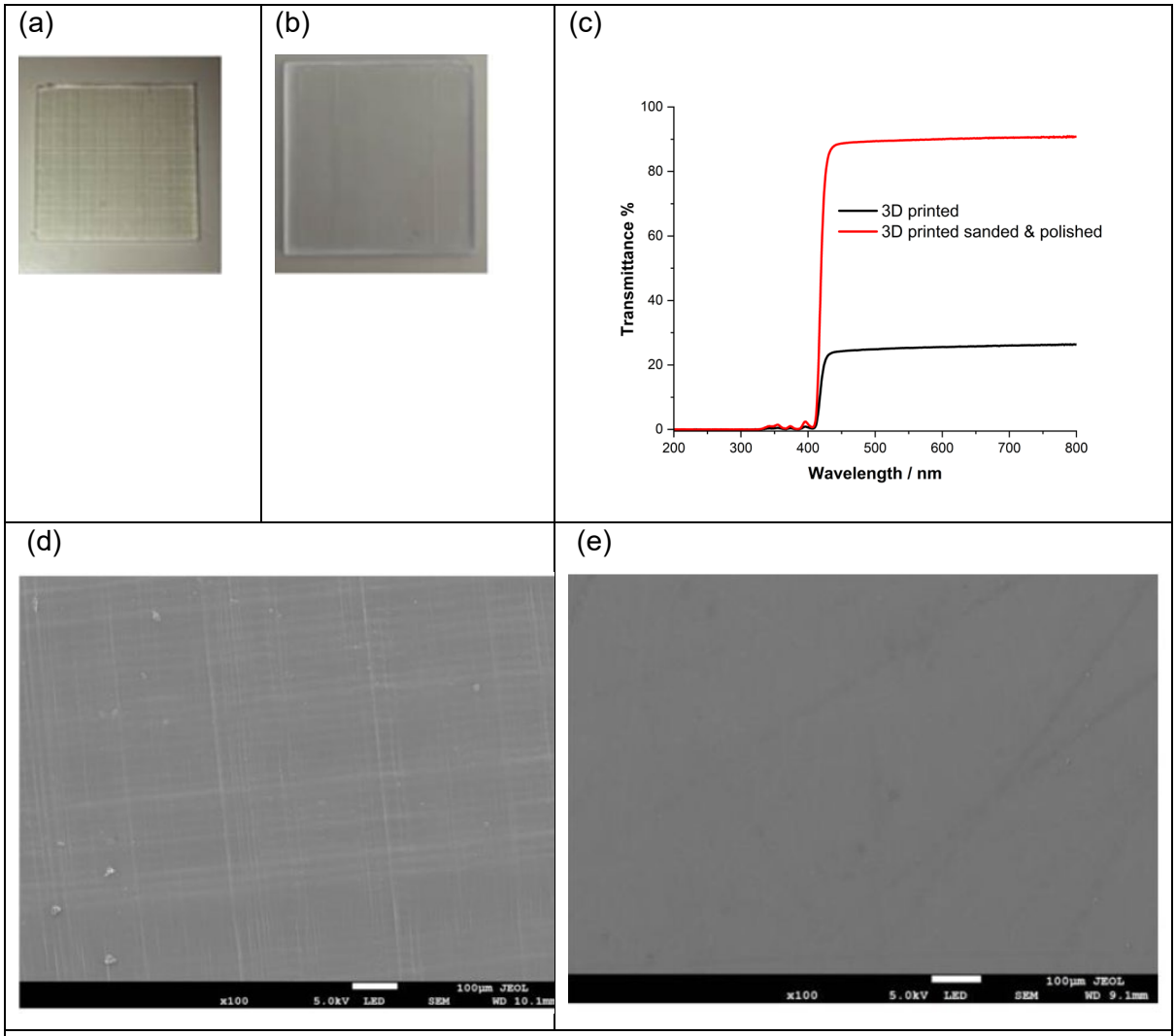

Figure 3. (a) Photo of a 3D printed blank LSC with no surface treatment, (b) Photo of a 3D printed blank LSC after sanding and polishing, (c) Graph of transmittance against wavelength showing the transparency improvement, (d) SEM image of a 3D printed blank LSC before surface treatment, ×100 magnification scale bar 100 µm, (e) SEM image of a 3D printed blank LSC after sanding and polishing ×100 magnification scale bar 100 µm.

To further investigate the effect of thickness and bulk scattering on optical performance, we fabricated blank 3D printed samples with thicknesses ranging from 1 mm to 5 mm and measured their transmission spectra (Fig. 4a). The results show that all samples maintain high transparency, with transmission values exceeding 85% in the visible range. We compare our results to a 4 mm thick Perspex sheet with recorded transmittance of ~92%. The observed drop in transmission with increasing thickness in the printed samples is consistent with minor bulk scattering, although the effect remains limited (Fig. 4b). These results support our conclusion that surface scattering remains the dominant loss mechanism, which can be substantially mitigated through surface treatment. Furthermore, we will

demonstrate that bulk scattering does not significantly impact the optical efficiency of the LSC, as evidenced by electrical characterisation and edge fluorescence measurements showing no appreciable loss in performance.

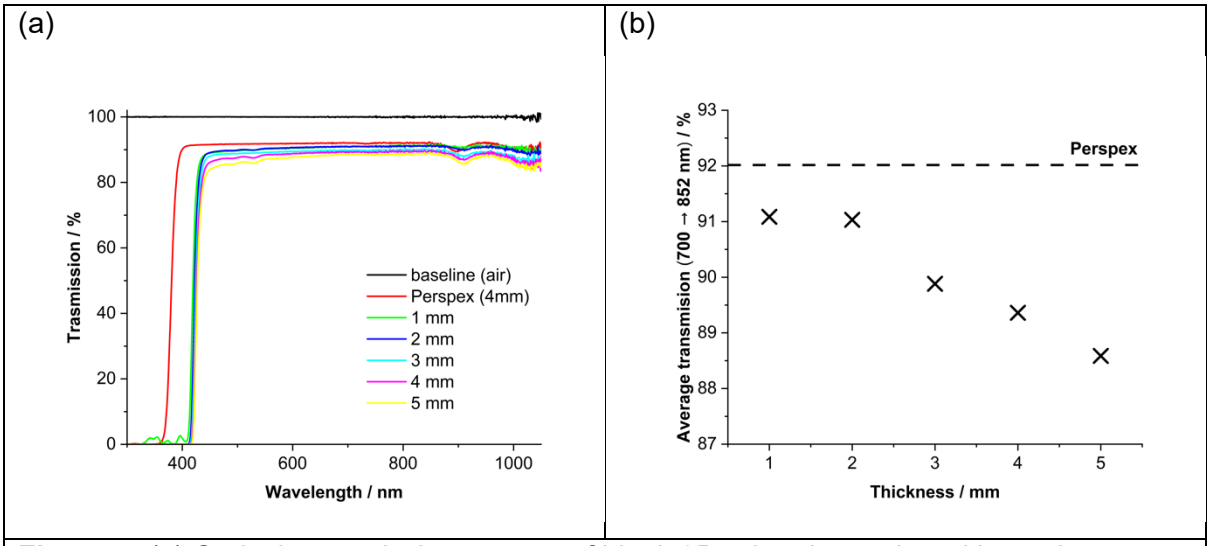

Figure 4. (a) Optical transmission spectra of blank 3D printed samples with varying thicknesses (1–5 mm), compared to a 4 mm thick Perspex reference and baseline (air). (b) Average optical transmission (700–852 nm) as a function of 3D printed sample thickness (1–5 mm). The dashed line indicates the reference transmission of a 4 mm Perspex sheet (~92%).

The next stage is to add the Pe-Red dye and make a 3D printed LSC for further optical and electrical characterisation measurements. Small 3D printed LSCs (2.0 cm × 2.0 cm × 0.1 cm) were fabricated to assess whether the addition of a luminophore to the clear resin would be successful as this process to our knowledge has not been reported in the literature before. An important consideration when designing LSCs is the gain factor [11].

This is the ratio of the area of the top face of the LSC which the photons enter the LSC to the combined area of the four edges of the LSC where light is concentrated to the four solar cells. Having a large gain factor is important for LSCs as it represents their main concentration function which is collecting light from a large area and concentrating it onto a smaller area. However, as the geometric gain increases, reabsorption and escape-cone losses also increase. We therefore set the dimensions of the 3D printed LSC to have a gain factor of 5 which is similar with current LSC research [10].

The concentration of the 3D printed Pe-Red LSC was chosen to be 0.3 g/L in order to compare with an injection moulded PMMA LSC that has been studied previously [34]. Figure 5a shows the absorption spectra for both the LSC plates that were tested in this work. The

IM LSC shows a slight blue shift with respect to the 3D printed LSC due to differences in the solvation. The IM LSC uses PMMA as the matrix material, whereas the 3D-printed LSC employs Clear Resin V4, a proprietary photopolymer primarily composed of UDMA with methacrylate monomers and a Diphenyl(2,4,6-trimethylbenzoyl)phosphine oxide photoinitiator. This resin exhibits optical properties very similar to PMMA, with a refractive index of approximately 1.51 across the visible range (400–700 nm), high transparency, and low scattering after polishing.

The absorbance maxima for the IM LSC and 3D LSC are 1.21 and 1.19 respectively, indicating that both samples exhibit very similar absorbance characteristics. We observed the onset of the absorption of the resin matrix in the 3D LSC below 410 nm. Figure 5b shows the measured edge fluorescence for the IM LSC, an untreated 3D LSC and a sanded/polished 3D LSC. The edge fluorescence spectra (600 nm – 800 nm) are indicative of the emitted spectrum from the edge of the LSC and is the spectral light that will illuminate the solar cells placed on the edges. We observed significant improvement (~64%) of the edge fluorescence intensity (660 nm) going from the untreated 3D printed LSC plate to the sanded and polished 3D LSC one.

The edge fluorescence of the IM LSC is comparable in intensity with the edge fluorescence of the 3D-printed LSC. The similarity in edge fluorescence spectra between the 3D printed and injection moulded LSCs indicates that bulk scattering in the printed material does not significantly impair photon transport to the edges. Although bulk scattering alters the trajectory of emitted light within the LSC, it does not necessarily lead to significant optical losses. This may explain the minimal performance loss observed in our edge fluorescence measurements. The blue LED illumination peak (465 nm) remained the same for the polished 3D-printed LSC and IM LSC signifying similar absorbance. The increased blue LED peak observed for the untreated 3D LSC is due to increased reflection/scattering and reduced absorbance.

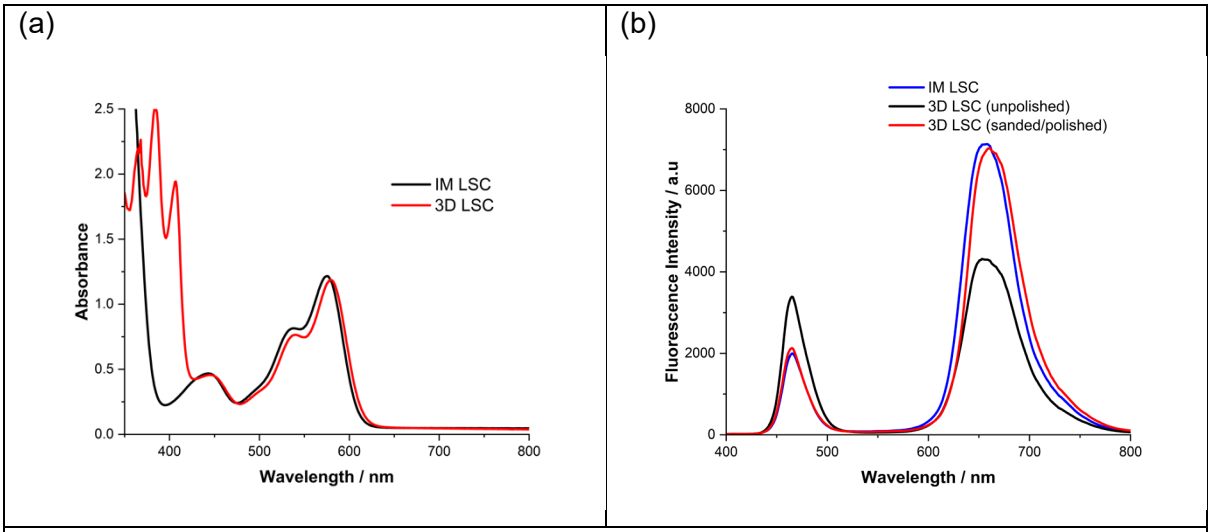

Figure 5. (a) Absorption spectra for an injection moulded Pe-Red LSC (0.3 g/L) and 3D printed LSC (0.3 g/L). (b)Edge fluorescence spectra for a polished Pe-Red LSC, unpolished Pe-Red LSC and an injection moulded LSC at the same concentration (0.3 g/L) with uniform illumination from a blue LED source (465 nm).

One of the key advantages of 3D printing is the ease with which the shape and size of LSCs can be modified, making it an ideal platform for rapid prototyping and experimental investigations in a research lab environment. We printed a series of different thickness (1.0 mm–5.0 mm) LSC plates of a known concentration (0.06 g/L) Pe-Red in the resin. The absorption spectra are shown in Figure 6a and a Beer-Lambert fit in Figure 6b. The molar absorption coefficient is 40,066 ± 131 M^{-1} cm^{-1} and is measured from a fit of absorbance (578 nm) as function of LSC plate thickness. This value matches well with the value obtained from Pe-Red toluene solutions as shown in Figure 2. Mixing the dye into the resin causes a 12% decrease in the absorption coefficient, which is to be expected as the solvent can influence the value of the molar absorption coefficient.

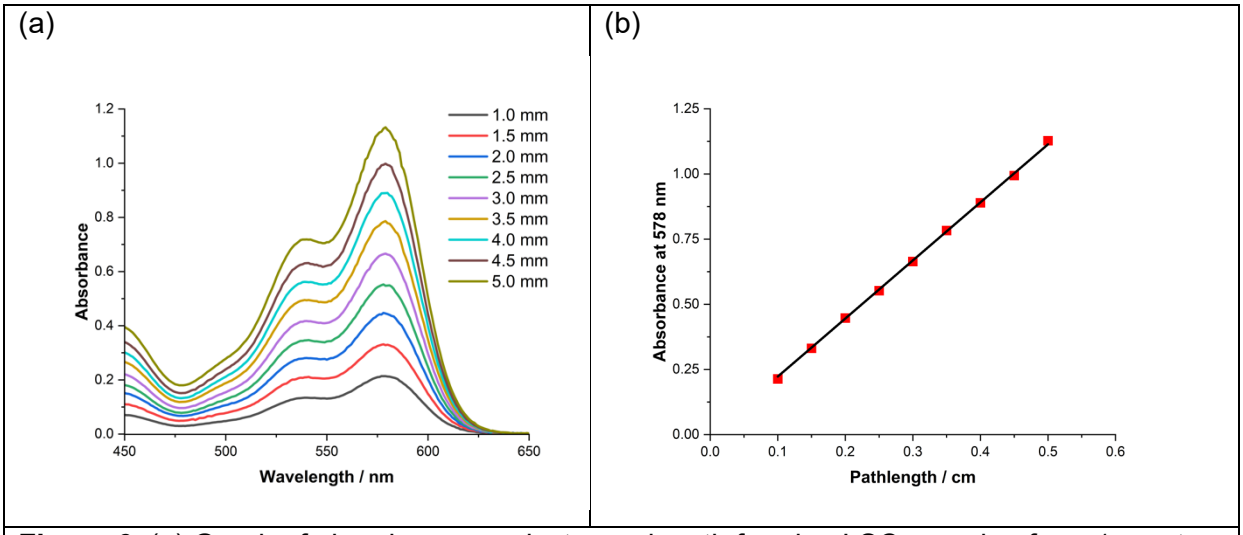

Figure 6. (a) Graph of absorbance against wavelength for nine LSCs ranging from 1 mm to 5 mm in thickness, (b) Beer Lambert plot of peak absorbance at 578 nm against path length.

3.2 Electrical Characterisation

Figure 7a shows the measured I–V curve of the small 3D-printed LSC (2.0 cm × 2.0 cm × 0.1 cm) doped with Pe-Red, compared with the IM LSC of identical dimensions (2.0 cm × 2.0 cm × 0.1 cm), both characterised under AM1.5G illumination. Figure 7b shows the experimental setup used for the measurements, illustrating the empty jig without an LSC in place. The maximum output power was measured as 2.82 ± 0.11 mW for the 3D-printed LSC and 2.72 ± 0.09 mW for the IM LSC, indicating very similar performance. The estimated power conversion efficiency (PCE) under AM1.5G illumination is 0.70% for both the 3D-printed and IM LSCs. These results demonstrate the viability of 3D printing for LSC fabrication and testing. Images of the IM and 3D-printed LSCs on the measurement jig are shown in Fig. 7c and Fig. 7d, respectively.

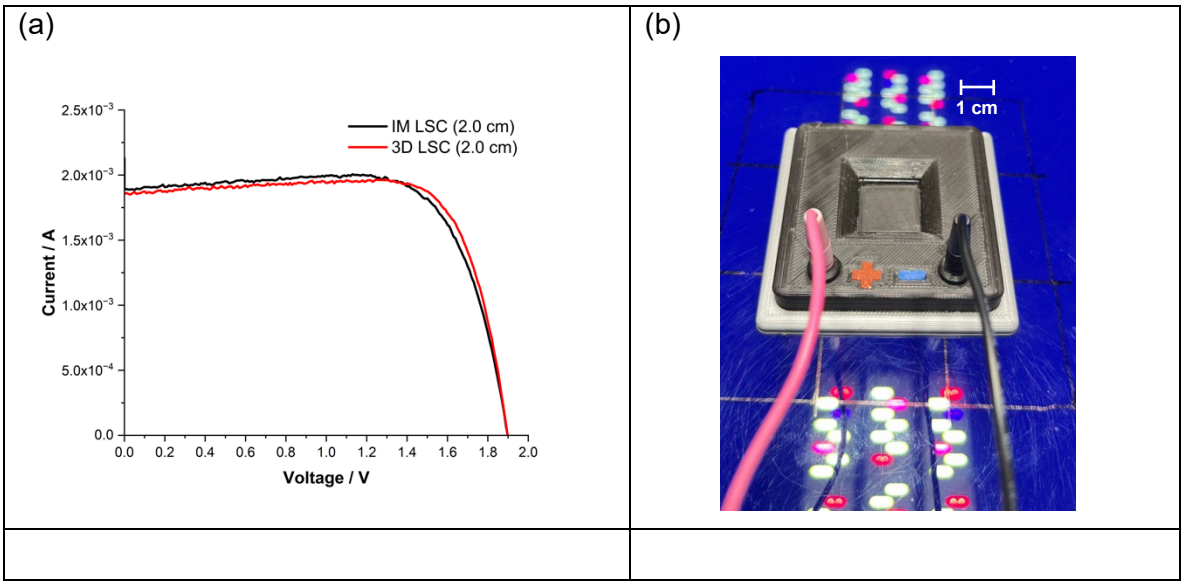

(c)

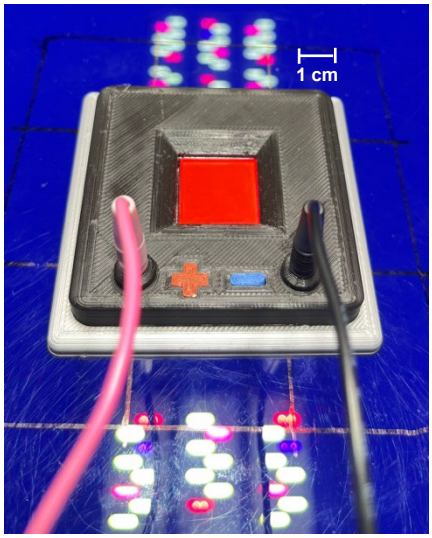

(d)

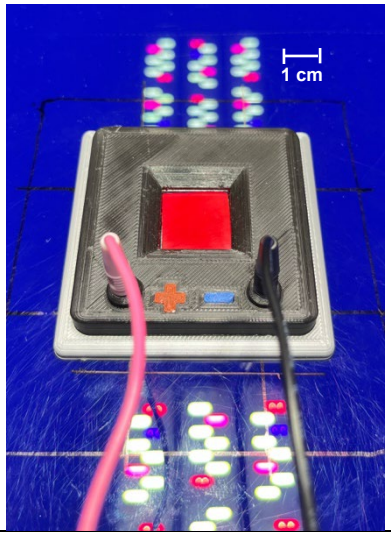

Figure 7. (a) Comparison of the current–voltage characteristics of the IM and 3D-printed LSCs (2.0 cm × 2.0 cm × 0.1 cm) under AM1.5G illumination. (b) Image of the measurement jig used for the electrical characterisation. (c) Image of the IM LSC and (d) image of the 3D-printed LSC placed on the measurement jig. Scale bar: 1 cm.

The encouraging results obtained with the small LSCs show comparable performance between the 3D-printed LSC and an IM LSC of similar Pe-Red concentration (0.3 g/L). The 3D printing was upscaled to evaluate a large LSC with dimensions (10.0 cm × 10.0 cm × 0.5 cm). The gain factor remained the same (gain=5) for both the small and the large LSC. The concentration was changed to 0.06 g/L by diluting the original dye-resin mixture by a factor of five. Higher efficiency solar cells (SunPower) were cut to size to complete the LSC device.

The I-V curve for the large 3D-printed LSC (10 cm × 10 cm × 0.5 cm) doped with Perylene Red at 0.06 g/L was recorded under white LED illumination (400–700 nm), which provided a larger and more uniform illumination area. As shown in Figure 8a, the device exhibited stable current-voltage behaviour with a maximum power output (P_{max}) of 7.60 mW and a fill factor (FF) of 0.66. The corresponding power conversion efficiency was 2.0%, as summarised in Table 1, which is comparable to values reported in the literature for single-dye LSC systems [41]. These results confirm that the large 3D-printed LSC, with solar cells optically coupled at the edges, demonstrates efficient light concentration and effective electrical performance under uniform illumination conditions. Further optimisation of the dye concentration and optical coupling conditions is expected to yield higher efficiencies in future designs.

(a)

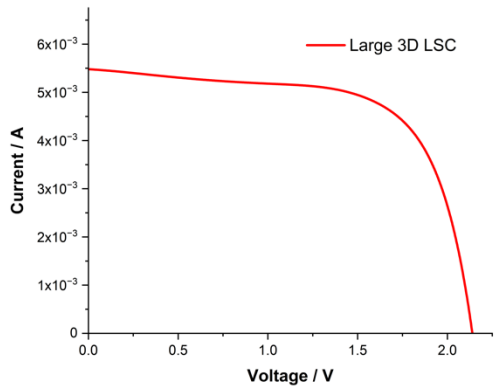

(b)

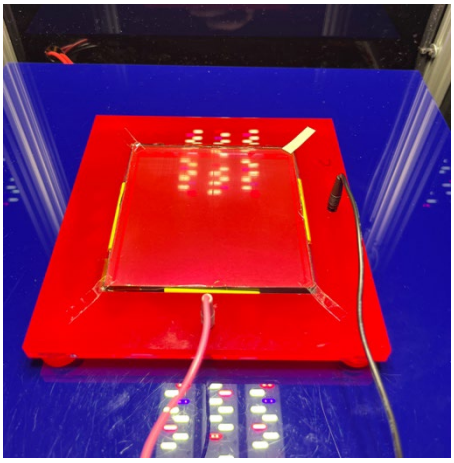

Figure 8. (a) Current-voltage characteristic of the large 3D-printed LSC (10 cm × 10 cm × 0.5 cm) doped with Perylene Red at a concentration of 0.06 g/L. (b) Photo of the custom-made large 3D-printed LSC placed on the measurement setup used for electrical characterisation under white LED illumination (400–700 nm).

Table 1. Electrical and optical performance parameters of optically coupled 3D-printed large (10 cm x 10 cm x 5 cm) LSC device for the Red (0.06 g/L) sample. Parameters include maximum power output (P_{max}), open-circuit voltage (V_{OC}), short-circuit current (I_{SC}), voltage and current at maximum power (V_{mp}, I_{mp}), fill factor (FF), device power conversion efficiency (η_{LSC-PV}).

LSC	P_{max} (mW)	V_{OC} (V)	I_{SC} (mA)	J_{SC} (mA cm^{-2})	V_{mp} (V)	I_{mp} (mA)	FF	Device Efficiency (η_{LSC-PV})
Red	7.60	2.10	5.48	0.05	1.66	4.58	0.66	2.0%

This work has demonstrated that stereolithography (SLA) 3D printing is well suited to the fabrication of LSC devices for research-led iteration of different geometries and formulations. At the highest Z-layer resolution (25 µm), individual LSCs were printed in ~4.5–5 h, while batches of 10–30 devices were produced within ~5–10 h, depending on the device footprint. Shorter print times are possible using coarser settings. Printer set-up takes a few minutes, printing can start after a 15 min warm-up period, and post-processing is completed within 20 min. This flexibility enables 3D printing to rapidly screen concentrations and geometries, supporting the development of laboratory-scale exemplars. By contrast, injection moulding, as the industry standard, can be used once the design and dye formulation have been finalised, offering tight tolerances, high repeatability, and very low cost per part at high

production volumes [42]. Its use at a research level for rapid prototyping and dye formulation screening can be limited by the cost and lead time of injection mould manufacture and optical cavity polishing [43]. Additional expenses are associated with post-tool design changes, as well as the time required for compounding, pelletising, and purging between different dye concentrations to avoid contamination [44]. Therefore, 3D printing enables rapid optimisation, while injection moulding provides a route to subsequent manufacturing scale-up.

4 Conclusions

This investigation reports, to the best of our knowledge, the first successful fabrication of luminescent solar concentrators (LSCs) doped with the widely used Perylene Red dye using stereolithography (SLA) 3D printing. The study demonstrates the potential of 3D printing as a practical and accessible method for research in LSC development. A two-step sanding and polishing process significantly enhanced the optical quality of the printed LSCs, achieving up to 90% transparency by effectively reducing surface scattering. The remaining bulk scattering was minimal, with measured transmission values exceeding 88% for 5 mm thick samples and approaching the 92% transmission benchmark of commercial Perspex. A small-scale 3D-printed LSC exhibited optical and electrical performance comparable to that of an injection-moulded counterpart with a similar dye concentration and gain factor. The method was successfully scaled up to fabricate a larger LSC, which confirmed the viability of SLA printing and demonstrated effective light concentration under blue LED illumination. A recorded power conversion efficiency of 2.0% under white LED illumination (400–700 nm) was obtained, which can be further improved through optimisation of the dye concentration. These results highlight SLA 3D printing as a promising platform for rapid, low-cost prototyping and optimisation of LSC devices in research settings.

Acknowledgements

The authors would like to thank Matthew Bentley for assistance with the AM1.5G measurements.

Conflict of Interest

The authors wish to declare no conflicts of interest.

Data Availability Statement

All data are available upon reasonable request from the corresponding author.

References

[1] W.H. Weber, J. Lambe, Luminescent greenhouse collector for solar radiation, Applied Optics 15 (1976) 2299. https://doi.org/10.1364/ao.15.002299.

[2] J.A. Levitt, W.H. Weber, Materials for luminescent greenhouse solar collectors, Applied Optics 16 (1977) 2684. https://doi.org/10.1364/ao.16.002684.

[3] B.A. Swartz, T. Cole, A.H. Zewail, Photon trapping and energy transfer in multiple-dye plastic matrices: an efficient solar-energy concentrator, Optics Letters 1 (1977) 73. https://doi.org/10.1364/OL.1.000073.

[4] A. Goetzberger, Fluorescent solar energy collectors: Operating conditions with diffuse light, Applied Physics 16 (1978) 399–404. https://doi.org/10.1007/BF00885865.

[5] P. Kittidachachan, L. Danos, T.J.J. Meyer, N.N. Alderman, T. Markvart, Photon Collection Efficiency of Fluorescent Solar Collectors, CHIMIA International Journal for Chemistry 61 (2007) 780–786. https://doi.org/10.2533/chimia.2007.780.

[6] T. Markvart, L. Danos, Edge-illuminated ultrathin crystalline silicon solar cell, in: Proceedings of 25th European Photovoltaic Solar Energy Conference and Exhibition, Valencia, 2010: pp. 5–6. https://doi.org/10.4229/25thEUPVSEC2010-2DV.1.89.

[7] T. Markvart, L. Danos, L. Fang, T. Parel, N. Soleimani, Photon frequency management for trapping & concentration of sunlight, RSC Advances 2 (2012) 3173–3179. https://doi.org/10.1039/c2ra01160c.

[8] I. Papakonstantinou, M. Portnoi, M.G. Debije, The Hidden Potential of Luminescent Solar Concentrators, Advanced Energy Materials 11 (2021) 1–13. https://doi.org/10.1002/aenm.202002883.

[9] A. Borja Block, J. Escarre Palou, M. Courtant, A. Virtuani, G. Cattaneo, M. Roten, H. Li, M. Despeisse, A. Hessler-Wyser, U. Desai, A. Faes, C. Ballif, Colouring solutions for building integrated photovoltaic modules: A review, Energy and Buildings 314 (2024) 114253. https://doi.org/10.1016/j.enbuild.2024.114253.

[10] B.S. Richards, I.A. Howard, Luminescent solar concentrators for building integrated photovoltaics: opportunities and challenges, Energy and Environmental Science 16 (2023) 3214–3239. https://doi.org/10.1039/d3ee00331k.

[11] J. Roncali, Luminescent Solar Collectors: Quo Vadis?, Advanced Energy Materials 10 (2020) 2001907. https://doi.org/10.1002/aenm.202001907.

[12] R.A.S. Ferreira, S.F.H. Correia, A. Monguzzi, X. Liu, F. Meinardi, Spectral converters for photovoltaics – What's ahead, Materials Today 33 (2020) 105–121. https://doi.org/10.1016/j.mattod.2019.10.002.

[13] M. Freunek Muller, Indoor Photovoltaics: Materials, Modeling, and Applications, Wiley, 2020.

[14] V. Pecunia, L.G. Occhipinti, R.L.Z. Hoye, Emerging Indoor Photovoltaic Technologies for Sustainable Internet of Things, Advanced Energy Materials 11 (2021). https://doi.org/10.1002/aenm.202100698.

[15] K. Seunarine, Z. Haymoor, M. Spence, G. Burwell, A. Kay, P. Meredith, A. Armin, M. Carnie, Light power resource availability for energy harvesting photovoltaics for self-powered IoT, J. Phys. Energy 6 (2024) 015018. https://doi.org/10.1088/2515-7655/ad1764.

[16] S.F.H. Correia, A.R.N. Bastos, M. Martins, I.P.E. Macário, T. Veloso, J.L. Pereira, J.A.P. Coutinho, S.P.M. Ventura, P.S. André, R.A.S. Ferreira, Bio-Based Solar Energy Harvesting for Onsite Mobile Optical Temperature Sensing in Smart Cities, Advanced Science 9 (2022) 2104801. https://doi.org/10.1002/advs.202104801.

[17] G. Figueiredo, S.F.H. Correia, B.P. Falcão, V. Sencadas, L. Fu, P.S. André, R.A.S. Ferreira, Multi-Surface Adhesion Luminescent Solar Concentrators for Supply-Less IoT, Advanced Science 11 (2024) 2400540. https://doi.org/10.1002/advs.202400540.

[18] H. Michaels, M. Rinderle, I. Benesperi, R. Freitag, A. Gagliardi, M. Freitag, Emerging indoor photovoltaics for self-powered and self-aware IoT towards sustainable energy management, Chem. Sci. 14 (2023) 5350–5360. https://doi.org/10.1039/D3SC00659J.

[19] M. Portnoi, P.A. Haigh, T.J. Macdonald, F. Ambroz, I.P. Parkin, I. Darwazeh, I. Papakonstantinou, Bandwidth limits of luminescent solar concentrators as detectors in free-space optical communication systems, Light Sci Appl 10 (2021) 3. https://doi.org/10.1038/s41377-020-00444-y.
[20] P. Xia, H. Sun, S. Xu, T. Zhou, S. Zong, C. Lu, C. Wang, Luminescent Solar Concentrators with Dual Functions of Photovoltaic and Piezoelectric Properties for Wireless Self-Powered Speed Measurement, Advanced Energy Materials 13 (2023) 2301332. https://doi.org/10.1002/aenm.202301332.
[21] L. Fang, T.S. Parel, L. Danos, T. Markvart, Photon reabsorption in fluorescent solar collectors, Journal of Applied Physics 111 (2012) 076104. https://doi.org/10.1063/1.3702815.
[22] D. Benetti, F. Rosei, Inorganic and Organic Nano-Emitters for Luminescent Solar Concentrators, ECS Meeting Abstracts MA2020-01 (2020) 1065–1065. https://doi.org/10.1149/MA2020-01161065mtgabs.
[23] Y. Li, P. Miao, W. Zhou, X. Gong, X. Zhao, N-doped carbon-dots for luminescent solar concentrators, J. Mater. Chem. A 5 (2017) 21452–21459. https://doi.org/10.1039/C7TA05220K.
[24] L. Danos, T.J.J. Meyer, P. Kittidachachan, L. Fang, T.S. Parel, N. Soleimani, T. Markvart, Chapter 9. Photon Frequency Management Materials for Efficient Solar Energy Collection, in: S.J.C. Irvine (Ed.), RSC Energy and Environment Series No. 12 Materials Challenges: Inorganic Photovoltaic Solar Energy, Royal Society of Chemistry, 2014: pp. 297–331. https://doi.org/10.1039/9781849733465-00297.
[25] B. Dzurnak, T. Markvart, Universal measure of photon collection efficiency of dye luminescent solar concentrators, Solar Energy Materials and Solar Cells 250 (2023) 112101. https://doi.org/10.1016/j.solmat.2022.112101.
[26] M. Buffa, S. Carturan, M.G. Debije, A. Quaranta, G. Maggioni, Dye-doped polysiloxane rubbers for luminescent solar concentrator systems, Solar Energy Materials and Solar Cells 103 (2012) 114–118. https://doi.org/10.1016/j.solmat.2012.04.019.
[27] M.D. Tyona, A theoritical study on spin coating technique, Advances in Materials Research 2 (2013) 195–208. https://doi.org/10.12989/amr.2013.2.4.195.
[28] G. Seybold, G. Wagenblast, New perylene and violanthrone dyestuffs for fluorescent collectors, Dyes and Pigments 11 (1989) 303–317. https://doi.org/10.1016/0143-7208(89)85048-X.
[29] Z.X. Low, Y.T. Chua, B.M. Ray, D. Mattia, I.S. Metcalfe, D.A. Patterson, Perspective on 3D printing of separation membranes and comparison to related unconventional fabrication techniques, Journal of Membrane Science 523 (2017) 596–613. https://doi.org/10.1016/j.memsci.2016.10.006.
[30] Ö. Keleş, C.W. Blevins, K.J. Bowman, Effect of build orientation on the mechanical reliability of 3D printed ABS, Rapid Prototyping Journal 23 (2017) 320–328. https://doi.org/10.1108/RPJ-09-2015-0122.
[31] S. Ebrahimisadr, B. Olyaeefar, S. Ahmadi-kandjani, Dual- luminophore efficient luminescent solar concentrator fabricated by low-cost 3D printing, Physica Scripta 98 (2023) 015833. https://doi.org/10.1088/1402-4896/acab8f.
[32] F. Alam, M. Elsherif, B. AlQattan, A. Salih, S.M. Lee, A.K. Yetisen, S. Park, H. Butt, 3D Printed Contact Lenses, ACS Biomater Sci Eng 7 (2021) 794–803. https://doi.org/10.1021/acsbiomaterials.0c01470.
[33] M. Hisham, A.E. Salih, H. Butt, 3D Printing of Multimaterial Contact Lenses, ACS Biomater. Sci. Eng. 9 (2023) 4381–4391. https://doi.org/10.1021/acsbiomaterials.3c00175.
[34] T.S. Parel, L. Danos, T. Markvart, L. Fang, Modeling photon transport in fluorescent solar concentrators, Progress in Photovoltaics: Research and Applications 23 (2014) 1357–1366. https://doi.org/10.1002/pip.2553.
[35] T.S. Parel, C. Pistolas, L. Danos, T. Markvart, Modelling and experimental analysis of the angular distribution of the emitted light from the edge of luminescent solar

concentrators, Optical Materials 42 (2015) 532–537. http://dx.doi.org/10.1016/j.optmat.2015.02.011.
[36] FormLabs, Optical properties of selected Formlabs SLA resins, (2025). https://support.formlabs.com/s/article/Optical-properties-of-selected-Formlabs-SLA-resins?language=en_US.
[37] C. Yang, H.A. Atwater, M.A. Baldo, D. Baran, C.J. Barile, M.C. Barr, M. Bates, M.G. Bawendi, M.R. Bergren, B. Borhan, C.J. Brabec, S. Brovelli, V. Bulović, P. Ceroni, M.G. Debije, J.-M. Delgado-Sanchez, W.-J. Dong, P.M. Duxbury, R.C. Evans, S.R. Forrest, D.R. Gamelin, N.C. Giebink, X. Gong, G. Griffini, F. Guo, C.K. Herrera, A.W.Y. Ho-Baillie, R.J. Holmes, S.-K. Hong, T. Kirchartz, B.G. Levine, H. Li, Y. Li, D. Liu, M.A. Loi, C.K. Luscombe, N.S. Makarov, F. Mateen, R. Mazzaro, H. McDaniel, M.D. McGehee, F. Meinardi, A. Menéndez-Velázquez, J. Min, D.B. Mitzi, M. Moemeni, J.H. Moon, A. Nattestad, M.K. Nazeeruddin, A.F. Nogueira, U.W. Paetzold, D.L. Patrick, A. Pucci, B.P. Rand, E. Reichmanis, B.S. Richards, J. Roncali, F. Rosei, T.W. Schmidt, F. So, C.-C. Tu, A. Vahdani, W.G.J.H.M. van Sark, R. Verduzco, A. Vomiero, W.W.H. Wong, K. Wu, H.-L. Yip, X. Zhang, H. Zhao, R.R. Lunt, Consensus statement: Standardized reporting of power-producing luminescent solar concentrator performance, Joule 6 (2022) 8–15. https://doi.org/10.1016/j.joule.2021.12.004.
[38] R.O. Al-Kaysi, T. Sang Ahn, A.M. Müller, C.J. Bardeen, The photophysical properties of chromophores at high (100 mM and above) concentrations in polymers and as neat solids, Physical Chemistry Chemical Physics 8 (2006) 3453–3459. https://doi.org/10.1039/b605925b.
[39] L.R. Wilson, B.S. Richards, Measurement method for photoluminescent quantum yields of fluorescent organic dyes in polymethyl methacrylate for luminescent solar concentrators, Applied Optics 48 (2009) 212–220. https://doi.org/10.1364/AO.48.000212.
[40] A. Kaniyoor, B. Mckenna, S. Comby, R.C. Evans, Design and Response of High-Efficiency, Planar, Doped Luminescent Solar Concentrators Using Organic-Inorganic Di-Ureasil Waveguides, Advanced Optical Materials 4 (2016) 444–456. https://doi.org/10.1002/adom.201500412.
[41] L. Desmet, A.J.M. Ras, D.K.G. De Boer, M.G. Debije, Monocrystalline silicon photovoltaic luminescent solar concentrator with 42% power conversion efficiency, Opt. Lett. 37 (2012) 3087. https://doi.org/10.1364/OL.37.003087.
[42] D. Kazmer, A.M. Peterson, D. Masato, A.R. Colon, J. Krantz, Strategic cost and sustainability analyses of injection molding and material extrusion additive manufacturing, Polymer Engineering & Science 63 (2023) 943–958. https://doi.org/10.1002/pen.26256.
[43] M. Speich, R. Börret, Mould fabrication for polymer optics, J. Eur. Opt. Soc.-Rapid Publ. 6 (2011) 11050. https://doi.org/10.2971/jeos.2011.11050.
[44] D. Török, T. Ageyeva, R. Boros, Á. Kovács, J.G. Kovács, Developing a method for evaluating color changeover in a hot-runner multi-cavity injection mold, Polymer Testing 115 (2022) 107759. https://doi.org/10.1016/j.polymertesting.2022.107759.